Characterization of an amplified piezoelectric actuator for multiple reference optical coherence tomography

SEAN O'GORMAN[1,*], KAI NEUHAUS[1], SERGEY ALEXANDROV[1], JOSH HOGAN[2], CAROL WILSON[2], PAUL M. MCNAMARA[1,4], AND MARTIN LEAHY[1,3]

[1] Tissue Optics and Microcirculation Imaging facility, National University of Ireland, Galway
[2] Compact Imaging, Inc. 897 Independence Ave., Suite 5B, Mountain View, CA 94043 USA
[3] Royal College of Surgeons, Dublin, Ireland
[4] Compact Imaging Ireland Ltd., Roselawn House, National Technology Park, Limerick, Ireland
[*] Corresponding author: s.ogorman2@nuigalway.ie

Compiled June 21, 2018

The characterization of an amplified piezoelectric actuator (APA) as a new axial scanning method for multiple reference optical coherence tomography (MR-OCT) is described. MR-OCT is a compact optical imaging device based on a recirculating reference arm scanning optical delay using a partial mirror that can enhance the imaging depth range by more than ten times of the reference mirror scanning amplitude. The scanning amplitude of the used APA was varied between 30 and 250 µm depending on the scanning frequency of between 0.8 and 1.2 kHz. A silver coated miniature mirror was attached to the APA via UV cured optical adhesive and the light source was a super-luminescent diode (SLED) with 1310 nm center wavelength and 56 nm bandwidth. The sensitivity was measured with and without the partial mirror in the reference delay line as a function of scan speed, frequency, and range, therefore, providing results for MR-OCT and TD-OCT modes. It was found that the APA provides more than twice of the mechanical scanning range compared to other opto-mechanic actuators but results indicate degradation of SNR and sensitivity at larger imaging depths. In conjunction with MR-OCT the scan range of maximum 200 µm can be enhanced up to 1 to 1.5 mm by using a reduced amount of orders of reflections which could be of interest to increase sensitivity in the future.

OCIS codes: 170.4500 Optical coherence tomography; (260.3060) Infrared; (060.2420)

http://dx.doi.org/10.1364/ao.XX.XXXXXX

1. INTRODUCTION

Optical coherence tomography (OCT) is a biomedical imaging technology that can obtain cross-sectional structural information with micrometer-scale resolution in depth [1]. Applications range from medical areas in ophthalmology allowing high-resolution imaging of the retina, iris, and cornea or highly scattering samples imaging of human skin among others. It is evident that portable and affordable OCT systems could support the increasing demand for preemptive health screening and point-of-care needs for future generations, and miniaturization efforts are experiencing fast-growing interest in science and industry. Notably, FD-OCT attracts most of the interest as it appears to be suitable for integrated photonic circuits and promises smallest form factor component designs [2, 3]. Another option that gains more and more interest is to use a simple miniature Michelson interferometer with a partial mirror in its reference arm. Such so-called multiple references optical coherence tomography (MR-OCT) system, owning its name from the multiple reference reflections originating from the partial mirror, can be designed from readily available and low-cost optomechanical components (Fig. 1). Consequently, the MR-OCT method can provide optimal scalability while achieving sufficient performance for low-spec hardware at low-costs and allows sufficient reduction in size depending on the application. The optical unit of an MR-OCT system with the size of a handheld device was already reported demonstrating the first step to build an operational unit with minimal efforts [4].

MR-OCT enhances the axial scan range in depth by more than ten times achieving more than 1 mm imaging depth compared to the otherwise shallow scan range of the optomechanical scan system used in the optical delay line of the Michelson interferometer. Other methods to overcome the shallow scan range of the optical delay line are using a stack of multiple mirror interfaces [5] which may cause problems due to the weight of the mirror stack. The physical principle of MR-OCT method is based on the recirculation of the reference wave using a static partial mirror which allows a reduced weight of the scanning mirror and higher scan frequencies [6]. Multiple different scanning system configurations were already reported including a piezo stack and a voice coil demonstrating the flexibility of the

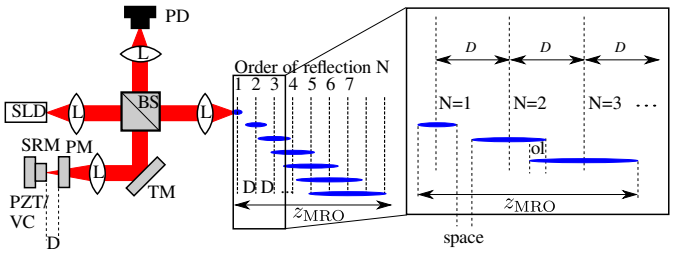

Fig. 1. Components: L: Lenses, SLD : super-luminescent diode, BS: beamsplitter, SRM: scanning reference mirror, PM: partial mirror, PD: photodetector PZT/VC: piezoelectric actuator (or voice coil) with reference mirror attached, TM: turning mirror. Seven scanned ranges in depth are indicated (blue) based on 7 order of reference reflections resulting in a total scan range z_{MRO}, and the spacing D between the SRM and PM. The "space" occurs due to the scan range to be smaller than the D as otherwise the SRM would touch the PM.

MR-OCT configuration [7–9].

For maximum scan rates so-called resonant scanners are described but depending on the application have limited scan amplitude [10] or required a multitude of further optical components [11]. The amplified resonant piezoelectric actuator (APA) from Thorlabs (PK2FSF1) was therefore of interest due to its specified scan amplitude of 220 µm at 1 kHz scan frequency.

2. METHODS

To characterize the interference signal using the APA, the sensitivity and SNR was measured for different operational conditions such as varying frequency, scan-amplitude, and the order of reference reflection N. The SNR and sensitivity were also measured in a TD-OCT configuration without the PM installed to obtain baseline values to compare with MR-OCT.

The APA was prepared using a silver-coated mirror with a diameter of 5 mm using UV curable adhesive (Norland, NOA 61). The mirror was positioned with a custom built fixture to achieve best axial alignment with emphasis on minimal cost implementation. The MR-OCT was equipped with an SLED from DenseLight (CS3207A) with a center wavelength of 1310 nm and a bandwidth of 56 nm. The SLED was coupled into the interferometer over fiber optics via an optical isolator and a final collimator.

To calculate the axial resolution of an OCT system, we know that the coherence length is inversely proportional to the light source bandwidth. A light source that has a broad spectral bandwidth has a short coherence length and hence better resolution. If the light source is assumed to have a Gaussian spectrum and line shape, we can estimate that the coherence length, l_c, is given by:

$$l_c = \frac{4ln2}{\pi}\frac{\lambda_0^2}{\Delta\lambda} \tag{1}$$

where λ_0 is the light source central wavelength and $\Delta\lambda$ is the full-width at half maximum (FWHM) [12**?**]. The axial resolution Δz is given by $l_c/2$ is then:

$$\Delta z = \frac{2ln2}{\pi}\frac{\lambda_0^2}{\Delta\lambda} \tag{2}$$

Because the axial resolution of an OCT system is decoupled from the transverse resolution, both values must be calculated and measured independently. The measured axial resolution of the system was measured with approximately 14 μm in air. The lateral resolution was calculated based on the sample lens parameters which determines the transverse beam diameter at the sample:

$$\Delta x = \frac{4\lambda_0}{\pi}\frac{f}{d} \tag{3}$$

Using lens parameters for diameter d = 3 mm and focal length f = 50 mm (Thorlabs AC254050C) and the center wavelength λ_0 = 1310 nm of the used light source the lateral resolution Δx was calculated with 27 µm.

The SNR was measured and calculated using:

$$\mathrm{SNR} = 20\log_{10}\left(\frac{P}{\sigma}\right) \tag{4}$$

where P is the peak of the envelope of the interference signal and σ is the RMS of the noise. The measurement was performed on the FFT of the interference signal in which case the spectral signal power and spectral noise power was used.

The sensitivity S was calculated based on the measured SNR by attenuating the sample arm with a neutral density filter (OD 2) and calculated:

$$S(N) = \mathrm{SNR}(N) + 2\times\mathrm{OD} \tag{5}$$

where OD corresponds to optical density value of 20 dB [13].

Each higher order interference signal will have a higher frequency related to the relative Doppler frequency due to the scanning mirror motion, and the reflection counts N. The motion of the SRM in the case of the amplified resonant piezo stack was assumed to behave closely to a spring-mass system in which case simple harmonic motion describes the time-dependent position and the velocity $v_z(t)$ and position $z(t)$ of the SRM can be calculated using:

$$z(t) = A\cos(\omega_{\mathrm{SRM}}t + \phi) \tag{6}$$

and

$$v_z(t) = A\omega_{\mathrm{SRM}}\sin(\omega_{\mathrm{SRM}}t + \phi) \tag{7}$$

with $\omega_{\mathrm{SRM}} = 2\pi f_{\mathrm{SRM}}$, A the scanning amplitude, and initial phase ϕ which is assumed to be zero.

The Doppler frequency in TD-OCT for a scanning mirror with linear motion $\bar{v}_M$ is calculated using:

$$f_D = \frac{2\bar{v}_M}{\lambda_0} \tag{8}$$

If we consider one half of the oscillation cycle ($\omega t = \pi$) for the scanning mirror, then the maximum Doppler frequency occurs at $\omega t = \pi/2$ in which case the sine function becomes unity, and the scanning mirror has a maximum velocity $\hat{v}_z(t) = 2A\pi f_{\mathrm{SRM}}$. Due to (8) the Doppler frequency is the maximum at $\hat{v}_z(t)$ and we can rewrite (8) for maximum values as $\hat{f}_D = 2\hat{v}_M/\lambda_0$. For each higher order N the maximum Doppler frequency is then calculated as:

$$\hat{f}_D(N) = \frac{4A\pi f_{\mathrm{SRM}}N}{\lambda_0} \tag{9}$$

It should be noted that after digitizing often the sinusoidal distortions of the interference signal are removed by digital processing and the frequency correlates to a linear mirror motion with constant velocity $\bar{v}_M = 2A/\Delta t$ and $\Delta t = 1/f_{\mathrm{SRM}}$. However, the peak frequency is of relevance to characterize the performance of the detector and detection electronics. The increase of the Doppler frequency of each higher order is expressed by simple

multiplication with a factor N based on the order number. This means the phase velocity is adding up for each reflection from the PM to the SRM velocity increasing the Doppler frequency by N.

Rearranging (9) the scanning range can be calculated based on the measured Doppler frequency

$$A = \frac{f_D \lambda_0}{4N\pi f_{\mathrm{SRM}}} \tag{10}$$

which is useful to investigate the scan range vs. the scan frequency f_{SRM}.

3. RESULTS

A. TD-OCT SNR and sensitivity

Multiple parameters such as peak sensitivity, SNR, resonance frequency, and sensitivity vs. scan range were measured for the ordinary time-domain mode, meaning the interferometer was operated without the PM in the reference arm.

The sensitivity of the TD system was characterized next. The sample arm was attenuated with an ND filter (OD2) and the reference arm power was adjusted with a variable ND filter. Multiple measurements for different reference arm powers were recorded to find the maximum sensitivity (Fig. 2) [13]. The uncertainty of the sensitivity values are indicated as error bars and indicate the repeatability of the measurements. The repeatability is of significance to understand the intermediate stability of the overall system, but should also be sensitive to changes in the scanning system. For example, we can expect that small changes in the spring characteristics should become visible in the change of sensitivity. The resonance characteristics of the actuator have

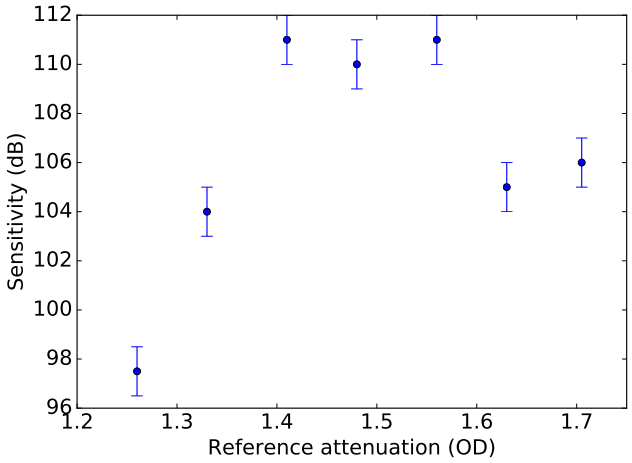

Fig. 2. Sensitivity of TD signal vs Reference attenuation (OD).

been measured (Fig. 3). The resonance frequency of the scanner with a mirror attached is approximately 975 Hz somewhat less than specified (1 kHz) due to the mirror mass which weighed approximately 5 grams. It was reported that with traditional non-resonant mechanical actuators (such as first voice coil actuator), the sensitivity degrades at a higher frequency due to a pointing instability at large scan ranges [14].

Figure 4 shows the dependency of the sensitivity vs. different scan frequencies. The scan range was kept constant in this TD configuration (without PM) to understand the effect of the scan

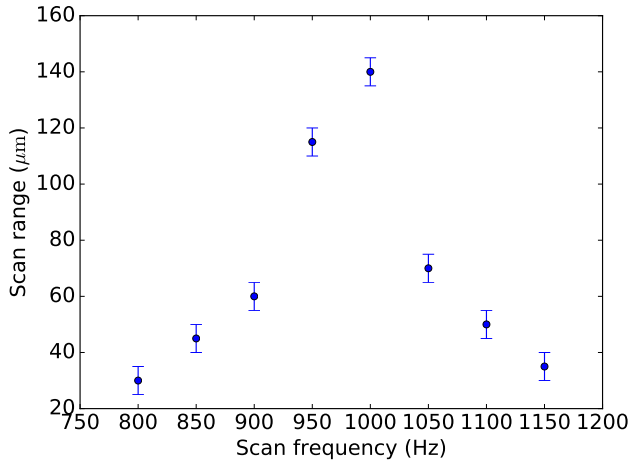

Fig. 3. Resonance curve of the scan range at different scan frequencies with constant voltage.

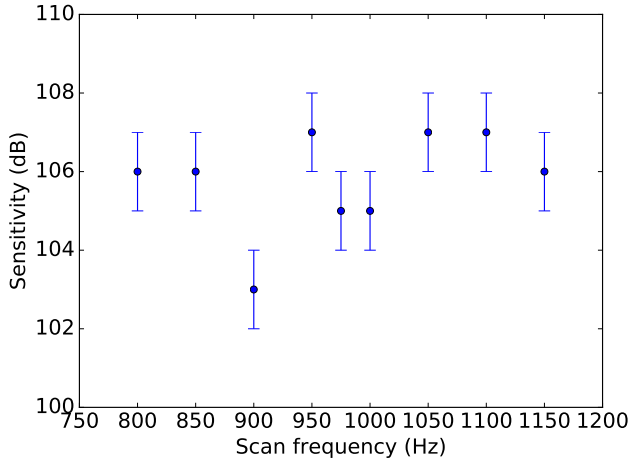

Fig. 4. Sensitivity measured at different frequencies with constant scan range (approx. 50 µm).

frequency that is not at resonance. Although the variation of sensitivity between 900 Hz and 950 Hz, which is close to the measured resonance point is larger than the estimated uncertainty, it is not sufficient yet to conclude if there is any significant effect visible.

Changing the scan range, however, does change the sensitivity (Fig. 5) which is expected due to the increasing pointing error of the SRM. Because the spring lever is subjected to larger forces at larger travel distances, non-isotropic material constants may become increasingly dominant causing deviations that affect the axial pointing of the SRM. Any axial pointing deviation of the SRM reduces the overlap of the reference and sample beam on the detector and consequently reduces the power of the interference signal and hence reduces the sensitivity.

B. MR-OCT SNR and sensitivity

For the MR-OCT configuration, a partial mirror with a splitting ratio 80/20 (CVI Melles Griot, PR1-1310-80-1025) was installed in front of the reference mirror with 80 percent reflectivity towards the scanning mirror. The sensitivity roll-off was measured for

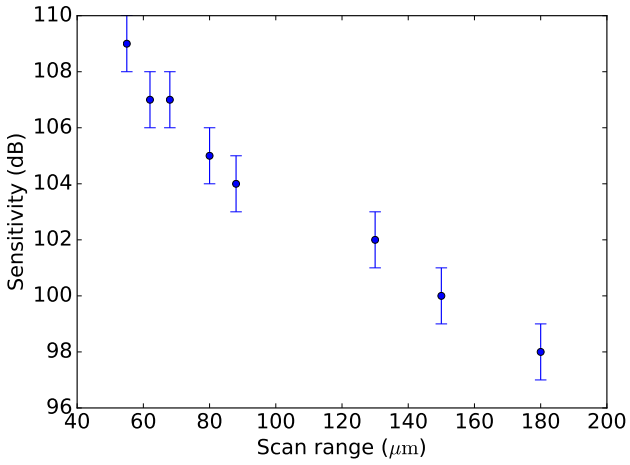

Fig. 5. Sensitivity measured at 975 Hz with increasing scan range.

ten orders of reflections (Fig. 6). The roll-off is determined by

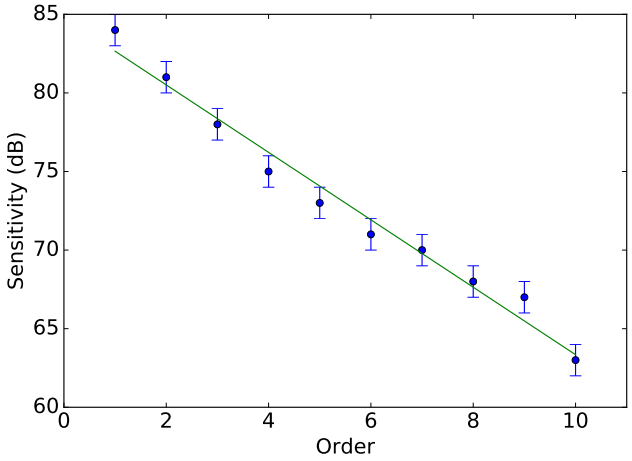

Fig. 6. Roll-off of sensitivity vs order.

the partial reduction of power for each higher order of reflection and has as expected linear characteristics. The measured slope of 2.1 dB is somewhat more substantial compared to previously published values [14].

The frequency stability describes the variation of the interference frequency for each higher order (Fig. 7). The importance of the frequency stability is related to the efficiency of filter performance based on the frequency bands and the ability to separate the signal for each order. The increasing variance of the frequencies will cause a washout in the image for higher orders of reflections.

4. COMPARATIVE SENSITIVITY MEASUREMENTS

The sensitivity of the APA was compared for the TD and MR-OCT vs. a first generation voice coil at 300 Hz (Fig. 8). The APA was actuated at less than its resonance frequency at about 950 Hz to reduce its scan range allowing for optimal placement of the PM. It was possible to tune the scan range to about 70 µm which

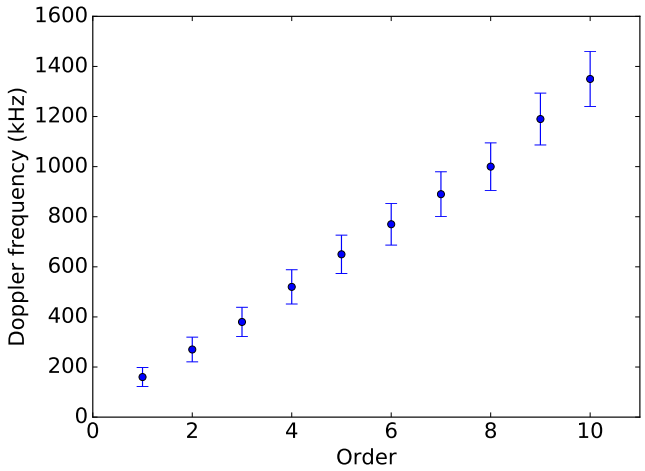

Fig. 7. Doppler frequency vs order.

severely affected the pointing accuracy of the SRM and consequently reduced the sensitivity. Due to the MR-OCT principle, a reengineering of the APA for shorter scan ranges at resonance could improve the sensitivity while the availability of higher orders would allow keeping the imaging depth constant.

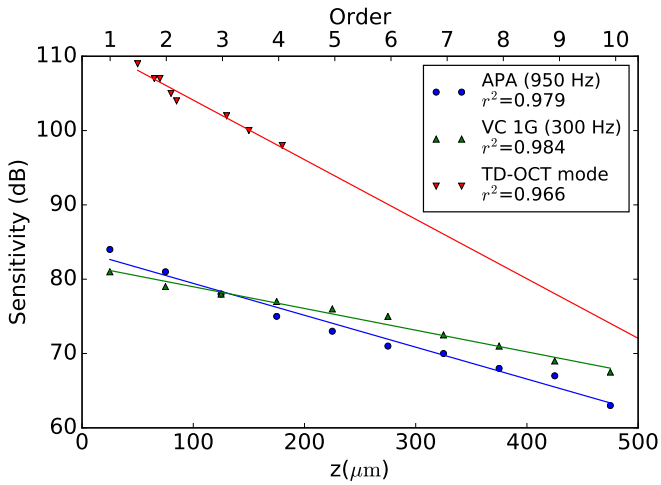

Fig. 8. Comparison of the APA in TD mode and MR-OCT mode at about 950 Hz vs. results of a first generation MR-OCT voice coil (VC 1G) at 300 Hz [14]. The roll-off for the TD mode of the APA spans about 200 µm as specified at resonance from about 110 dB sensitivity. To allow proper placement of the PM, the scan range was reduced, by operating off resonance, which resulted in a lower sensitivity. However, the sensitivity of the APA matches that of a first generation VC at three times the scan speed.

5. CONCLUSIONS AND FUTURE WORK

The characterization of an amplified resonant piezo actuator (APA) for the reference delay line of an MR-OCT system was described. The current results indicate that at larger scan ranges the axial pointing error of the scan axis of the SRM is significantly

reducing the sensitivity of higher orders. The measured sensitivity for the first order was 85 dB and the roll-off was 2.1 dB. The strong roll-off causes a significant reduction of sensitivity of higher orders which currently limits the imaging capabilities using the selected APA. It can be hypothesized that a purpose build resonant scanner with less scan range could provide better pointing stability which can improve the roll-off and hence conceivably the image quality in scattering samples. So far the investigated APA can be still of interest for applications to image weak scattering samples. A follow-on study can investigate the increase of the SRM to PM spacing such that the orders with higher sensitivity are projected to layers of interest which could be used to image the retina of the eye [15]. Another aspect demonstrated in this study was the relatively simple modification of the scanning system of the delay line of the interferometer for MR-OCT which allows a broader range of applications compared to other OCT systems.

FUNDING

This work was supported by NUI Galway, Galway University Foundation, the University of Limerick Foundation, the National Biophotonics Imaging Platform (NBIP) Ireland funded under the Higher Education Authority PRTLI Cycle 4, co-funded by the Irish Government and the European Union - Investing in your future, and Compact Imaging, Inc.

DISCLOSURES

The TOMI group at NUI Galway has received research support from Compact Imaging, Inc. All authors have a financial interest in Compact Imaging, Inc. and the intellectual property of MR-OCT.

ACKNOWLEDGMENTS

Sincere gratitude to my co-authors for their valuable insight and discussions about our shared research interests.

REFERENCES

1. D. Huang, E. Swanson, C. Lin, J. Schuman, W. Stinson, W. Chang, M. Hee, T. Flotte, K. Gregory, C. Puliafito, and a. et, Science **254**, 1178 (1991).
2. R. G. Hunsperger, *Integrated Optics: Theory and Technology* (Springer Science & Business Media, 2002).
3. J. M. Zara, S. Yazdanfar, K. D. Rao, J. A. Izatt, and S. W. Smith, Opt. Lett. **28**, 628 (2003).
4. P. M. McNamara, R. Dsouza, C. O'Riordan, S. Collins, P. O'Brien, C. Wilson, J. Hogan, and M. J. Leahy, J. Biomed. Opt. **21**, 126020 (2016).
5. R. Sharon, R. Friedman, and I. Abdulhalim, Opt. Commun. **283**, 4122 (2010).
6. J. N. Hogan, "Multiple Reference OCT System," (2013). US9113782B2.
7. R. Dsouza, H. M. Subhash, K. Neuhaus, J. Hogan, C. Wilson, and M. Leahy, Appl Opt **54**, 5634 (2015).
8. R. Dsouza, H. Subhash, K. Neuhaus, R. Kantamneni, P. M. McNamara, J. Hogan, C. Wilson, and M. Leahy, Lasers Surg. Med. **48**, 77 (2016).
9. R. Dsouza, H. Subhash, K. Neuhaus, J. Hogan, C. Wilson, and M. Leahy, Biomed. Opt. Express **5**, 2870 (2014).
10. B. M. Hoeling, M. E. Peter, D. C. Petersen, and R. C. Haskell, Rev. Sci. Instruments **75**, 3348 (2004).
11. X. Liu, M. J. Cobb, and X. Li, "Optics letters" **29** (2004).
12. Y. Pan, R. Birngruber, J. Rosperich, and R. Engelhardt, Appl. Opt. **34**, 6564 (1995).
13. R. Leitgeb, C. K. Hitzenberger, and A. F. Fercher, Opt. Express **11**, 889 (2003).
14. R. I. Dsouza, "Towards Low Cost Multiple Reference Optical Coherence Tomography for in Vivo and NDT Applications," Thesis, National University of Ireland, Galway (2016).
15. K. Neuhaus, S. O'Gorman, P. M. McNamara, S. A. Alexandrov, J. Hogan, C. Wilson, and M. J. Leahy, JBO, JBOPFO **22**, 086006 (2017).